Korean J. Chem. Eng., 39(7), 1880-1890 (2022)
DOI: 10.1007/s11814-022-1104-5

pISSN: 0256-1115
eISSN: 1975-7220

Evaluation of folic acid-conjugated chitosan grafted Fe_3O_4/graphene oxide as a pH- and magnetic field-responsive system for adsorption and controlled release of gemcitabine

Arsalan Ashuri, Mahsasadat Miralinaghi†, and Elham moniri

Department of Chemistry, Faculty of Science, Varamin - Pishva Branch, Islamic Azad University, Varamin, Iran
(*Received 16 December 2021 • Revised 4 March 2022 • Accepted 9 March 2022*)

Abstract−A pH-responsive system was prepared by using a magnetic nanocomposite, folic acid-conjugated chitosan (FA-CS) grafted Fe_3O_4/GO, and then used for loading and controlled release of an anti-cancer drug, gemcitabine (GEM). The successful synthesis of FA-CS/Fe_3O_4/GO was confirmed by various characterization techniques such as FE-SEM/EDX, TEM, FT-IR, XRD, TGA, VSM, and BET. The nanocomposite had a mesoporous structure with the specific surface area of 68.96 $m^2\ g^{-1}$, the pore volume of 0.25 $cm^3\ g^{-1}$, and the mean pore size of 14.78 nm. The optimum conditions for drug loading through adsorption were found to be pH=4, adsorbent dosage of 0.5 g L^{-1}, temperature of 298 K, and contact time of 45 min. Experimental data indicated that GEM adsorption onto FA-CS/Fe_3O_4/GO has a satisfactory correlation with the pseudo-second-order kinetic and Freundlich isotherm equations. The maximum adsorption capacity of GEM was 221.17 mg g^{-1} for FA-CS/Fe_3O_4/GO, which was quite higher than the non-functionalized Fe_3O_4/GO with the value of 33.99 mg g^{-1}. Furthermore, the *in-vitro* drug release profile of GEM from drug-loaded FA-CS/Fe_3O_4/GO was studied within 48 hours at 37 °C, and the results indicated a higher drug cumulative release amount in simulated cancer fluid (pH 5.6) compared to simulated human blood fluid (pH 7.4). Also, the Peppas-Sahlin kinetic model best fitted the release kinetics data. The result of drug release implied that FA-CS/Fe_3O_4/GO magnetic biocomposite could be a potential carrier for the sustained and controlled release of GEM.

Keywords: Gemcitabine, Isotherm, Release Kinetics, Smart Nanocarrier, Chitosan

INTRODUCTION

Nanotechnology has recently attracted a great deal of interest due to its ability to effectively diagnose and treat various tumors [1,2]. The common problems associated with conventional anti-tumor drug release systems include non-selectivity, severe side effects, a fast release profile, and damage to normal cells. In this regard, new drug delivery systems have been developed based on nanocarriers, which are also known as smart drug delivery systems (SDDs) [2-4]. These systems are capable of carrying and releasing the drug at the proper concentration at the targeted site under external or internal stimulation. In this way, they can improve the bioavailability and therapeutic efficacy of the anti-tumor agents while decreasing their side effects. The toxicity of nanocarriers is the main obstacle to the success of SDDs. Some studies have addressed the optimization of the toxicity of currently available nanocarriers or developing new nanocarriers with lower toxicity [3,5].

Recently, GO has been widely considered in the areas of drug delivery, biosensing, bioimaging, and phototherapy due to its water solubility, facile chemical modification, biocompatibility, high optical absorbance in the NIR region, low cost, abundance, and long circulation time in the blood [6]. Various compounds have been employed to modify the GO surface to design the controlled drug release systems responding to environmental stimuli, for instance pH, temperature, redox potential, light, enzyme, and external magnetic field. Among these stimuli, sensitivity to external magnetic field and pH is of crucial significance for the design of smart drug delivery devices [7-9].

The extracellular environment around the tumor tissues has an acidic pH, making it a proper stimulation for drug release [3]. Chitosan is a natural polysaccharide polymer with superior biodegradability, bio-availability, and biocompatibility that can be protonated at acidic pH values, resulting in de-polymerization [10,11]. Therefore, chitosan is a safe and excellent pH-responsive coating [9,12]. Fe_3O_4 nanoparticles can also be employed for the preparation of particles responsive to external magnetic fields [13]. These nanocarriers can be utilized for directing and accumulating drugs into tumor tissue cell by means of a magnetic field. Furthermore, modification of the carriers with ligands capable of binding to specific tumor cells is a well-known strategy to develop targeted drug release systems. Folic acid (FA) has a high affinity for folate receptors whose activity and quantity are significantly higher on the tumor cell membrane than that on the normal ones. FA can be a promising candidate as the targeted ligand [10,14].

Kim et al. developed FA-conjugated CS functionalized GO (FA-CS-GO) as a multifunctional nanoplatform that has a high photothermal efficiency and good near-infrared fluorescence/photoacoustic imaging ability [9]. The *in-vitro* cytotoxicity of FA-CS-GO against human breast cancer MDA-MB-231 cells was evaluated by MTT assay. According to the obtained results, the viability of MDA-MB-

†To whom correspondence should be addressed.
E-mail: msmiralinaghi@gmail.com, m_miralinaghi@iauvaramin.ac.ir

231 cells remained above 65%, which confirmed the low cytotoxicity and high biocompatibility of FA-CS-GO against MDA-MB-231 cells. Also, magnetic halloysite nanotubes trifunctionalized with FA, CS, and CPT medication have been applied as a dual-targeted drug nanocarrier to deliver camptothecin (CPT) into human epithelial colorectal adenocarcinoma cells (Caco-2), showing a strong cell growth inhibitory effect against the Caco-2 cancer cells [15]. However, the cytotoxicity of the blank nanocomposites (FA-COS/MHNTs) was negligible even under the high concentration of 1,000 μg mL^{-1} due to the high cell viability, which was approximately 81%.

Despite a number of previous studies, the field of multi-stimuli responsive drug delivery systems is still at its earliest stages, and the design of stimuli-responsive materials for controlled release is being incessantly researched in order to move it from the bench to the clinic. Hence, a multi-stimuli-responsive and tumor-targeted system that can be attained by integrating the advantages of biopolymer CS, FA ligand conjugation, and magnet directing could interactively improve the helpful effectiveness of graphene-based vehicles. Chemotherapeutical drugs such as gemcitabine (GEM) [16], CPT [17,18], doxorubicin [19,20], cisplatin [16], paclitaxel [21], and curcumin [22] can be conjugated to the GO composites containing FA.

GEM (2′,2′-difluoro-2′-deoxycytidine; dFdC) is a fluorinated nucleoside analog (NA) widely used in clinical practice for the treatment of several solid tumors, such as non-small cell lung, ovarian, bladder, thyroid, ovarian, pancreatic, breast, and multiple myelomas. In this study, FA-CS/Fe_3O_4/GO was successfully prepared as a pH- and magnetic field-responsive nanocarrier. GEM was selected as an anti-cancer drug to study the performance of FA-CS/Fe_3O_4/GO in drug loading and drug release in the simulated human blood fluid and cancer fluid. Moreover, non-linear adsorption isotherms, kinetics, and release kinetics were also conducted to better understand the mechanism of adsorption and *in-vitro* release.

MATERIALS AND METHODS

1. Materials

The GEM ($C_9H_{11}F_2N_3O_4$) drug was provided by Arasto Pharmaceuticals Co. (Iran, Tehran). CS ($C_{56}H_{103}N_9O_{39}$), FA ($C_{19}H_{19}N_7O_6$), dimethyl sulfoxide (DMSO, C_2H_6OS), 1-ethyl-3-(3-dimethylaminopropyl) carbodiimide (EDC, $C_8H_{17}N_3$), disodium hydrogen phosphate (Na_2HPO_4), sodium dihydrogen phosphate (NaH_2PO_4) were all bought from Merck (Darmstadt, Germany). N-hydroxysuccinimide (NHS, $C_4H_5NO_3$), iron (III) chloride hexahydrate ($FeCl_3{\cdot}6H_2O$), and iron (II) chloride tetrahydrate ($FeCl_2{\cdot}4H_2O$) were provided from Sigma Aldrich, USA. A stock standard solution of the GEM was prepared with deionized water and used for the preparation of the GEM working solutions by dilution.

2. GEM Carrier Preparation

2-1. Preparation of Magnetic Graphene Oxide (Fe_3O_4/GO)

GO was synthesized by the oxidation of expandable graphite similar to the ultrasound-assisted Hummers method [23]. Magnetic GO (Fe_3O_4/GO) was prepared by dissolving 6.8 g of $FeCl_3{\cdot}6H_2O$ and 3.5 g of $FeCl_2{\cdot}4H_2O$ into 250 mL solution containing 1 g of fully-dispersed GO under N_2 atmosphere, and heating to 358 K for 30 min. Subsequently, ammonia solution (20 mL) was added dropwise into the mixture to bring the pH value to 10. Then, the resulting reaction mixture was refluxed under the same conditions for another 60 min. After being cooled to room temperature, the black Fe_3O_4/GO sediment was collected, rinsed sequentially with deionized water and ethanol, and then dried under vacuum at 323 K [24].

2-2. Preparation of Folic Acid-Conjugated Chitosan (FA-CS)

To conjugate FA on CS, 0.15 g of FA dispersed in 250 mL of anhydrous DMSO was poured into a conical flask at room temperature and mechanically stirred for 60 minutes. Next, the reaction solution was activated by a known amount of EDC and NHS (a mass ratio of 1 : 2) and then added slowly to the CS solution (0.5% w/v) in 100 mL of acetic acid solution (0.1 M). The mixture was further agitated for 16 hours at room temperature under dark conditions (to avoid photo-degradation of FA). Following that, an appropriate amount of aqueous NaOH (0.1 M) was charged to the solution to adjust the pH value to 9. After centrifuging, the yellow precipitate was separated, then fully dispersed into 10 mL of distilled water and dialyzed against PBS solution for three days. Finally, the FA-CS was collected by centrifugation and freeze-dried [13]. Fig. S1 in the supplementary material illustrates the schematic of the FA-CS synthesis.

2-3. Preparation of FA-CS Grafted Magnetic GO (FA-CS/Fe_3O_4/GO)

First, 0.1 g of FA-CS was dissolved in acetic acid (20 mL) under constant stirring conditions for 24 h. The prepared Fe_3O_4/GO was dispersed in 20 mL of ethanol and placed in an ultrasonic bath for 3 h. Next, FA-CS solution (20 mL) was charged to the above suspension and agitated for a day at room temperature. The final product, FA-CS/Fe_3O_4/GO, was recovered using a permanent magnet, freeze-dried, and stored in the desiccator [9]. Fig. 1 displays the schematic illustration of (a) the synthesis root of FA-CS/Fe_3O_4/GO and (b) GEM loading.

3. Characterization Techniques

Details about the characterization techniques of materials are available in the supplementary material.

4. GEM Adsorption Tests

To carry out the experiments, first, a precise amount of the synthesized FA-CS/Fe_3O_4/GO was dispersed into the 20 mL of GEM solution with the specified concentration in an Erlenmeyer flask. The pH values of the GEM solutions were adjusted by adding a small volume of NaOH (0.01 M) or HCl (0.1 M) solution. Subsequently, the obtained mixture was stirred for specific time intervals on a water bath shaker at 200 rpm at a given temperature. At the fixed times, the adsorbent was separated by a magnetic field and the remaining GEM concentration was immediately measured at the maximum absorption wavelength (λ_{max}) of 269 nm by using a UV-Vis spectrophotometer. Eq. (1) was applied to calculate the adsorption capacity (q_t) of GEM:

$$q_t = \frac{(C_0 - C_t)V}{m} \quad (1)$$

where C_0 (mg L^{-1}) and C_t (mg L^{-1}) represent GEM concentration at zero and time t, in the respective order. V (L) and m (g) are the volume of GEM solution and the mass of FA-CS/Fe_3O_4/GO.

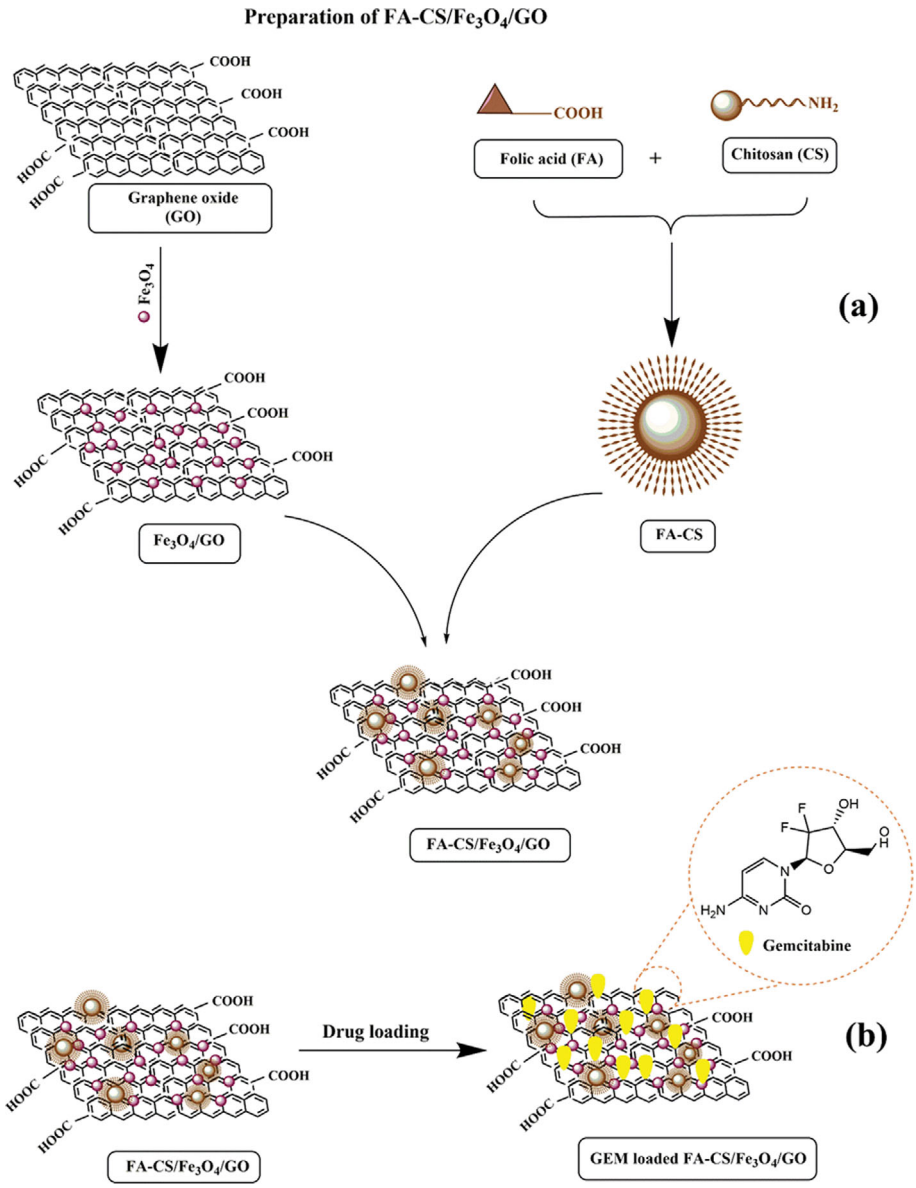

Fig. 1. (a) Schematic illustration of the synthesis root of FA-CS/Fe_3O_4/GO and (b) GEM loading.

5. Isotherm and Kinetic Adsorption Studies

To explore the mechanism of the adsorption procedure through an isotherm study, 10 mg of FA-CS/Fe_3O_4/GO was added to 20 mL solutions containing (2-120 mg L^{-1}) of GEM in the Erlenmeyer flask and stirred for 90 min at four temperatures in the range of 298-333 K [25]. Four isotherm models, namely, Langmuir [26], Freundlich [27], Temkin, [28] and Dubinin-Radushkevich (D-R) [29], were applied to fit the equilibrium data. The nonlinear forms of the aforementioned models are expressed by Eqs. (2)-(5), respectively.

$$q_e = \frac{q_{max} K_L C_e}{1 + K_L C_e} \quad (2)$$

$$q_e = K_F C_e^{1/n} \quad (3)$$

$$q_e = \frac{RT}{b} \ln(A_T C_e) \quad (4)$$

$$q_e = q_S e^{-B\varepsilon^2} \quad (5)$$

where q_e (mg g^{-1}), q_{max} (mg g^{-1}), C_e (mg g^{-1}), and K_L (L mg^{-1}) represent the equilibrium adsorption capacity, maximum adsorption capacity, the equilibrium GEM concentration, and Langmuir constant, respectively; K_F ($mg^{1-\frac{1}{n}} L^{\frac{1}{n}} g^{-1}$) and n show Freundlich isotherm constant and the heterogeneity factor, respectively; A_T (L mg^{-1}) and b (J g mol^{-1} mg^{-1}) are Temkin constant linked to equilibrium binding energy and adsorption heat, respectively; R (8.314 J mol^{-1} K^{-1}) and T (K) are the gas constant and the temperature, in the respective order; B (mol^2 J^{-2}) and q_S (mg g^{-1}) denote Dubinin-Radushkevich isotherm constant, and the theoretical adsorption capacity, respectively; ε is Polanyi potential defined as $\varepsilon = RT \ln[1+1/C_e]$. The average free energy of adsorption (E (kJ mol^{-1})) can be assessed from B value, as $E = 1/(2B)^{1/2}$.

To investigate the kinetic study, the experiments were fulfilled at pH 4 and GEM concentration of 20 mg L^{-1} with three adsorbent dosages (5-20 mg) at room temperature. The solutions were stirred for 2-75 min. The dynamic experimental results were conducted at the pseudo-1st-order (PFO) [30], pseudo-2nd-order (PSO) [31], Elovich [32], and fractional power (FP) [33] kinetic models to analyze the adsorption rate of GEM onto FA-CS/Fe_3O_4/GO [34,35]. The nonlinear forms of the aforementioned models are expressed by Eqs. (6)-(9), respectively.

$$q_t = q_e(1-e^{-k_1 t}) \tag{6}$$

$$q_t = \frac{k_2 q_e^2 t}{1+k_2 q_e t} \tag{7}$$

$$q_t = \frac{1}{\beta}\ln(\alpha\beta t) \tag{8}$$

$$q_t = at^b \tag{9}$$

where q_t (mg g^{-1}) is the instantaneous adsorption capacity; k_1 (min^{-1}) and k_2 (g mg^{-1} min^{-1}) denote the rate constant of GEM adsorption in PFO and PSO kinetic models, respectively; α (mg $g^{-1}min^{-1}$) represents the initial adsorption rate constant and β (g mg^{-1}) is the desorption constant; a (mg $g^{-1}min^{-b}$) and b are FP rate constant and power of the FP model, respectively.

6. GEM *In-vitro* Release Tests

For the preparation of the drug carrier, 0.2 g of FA-CS/Fe_3O_4/GO (Fe_3O_4/GO) was suspended in a 50 mL aqueous solution of GEM (80% v/v) with a concentration of 500 mg L^{-1}, followed by adjusting the pH level at 4.0. After a continuous shaking for 60 min at room temperature and 300 rpm, the resulting carrier was taken out and washed to remove the unloaded drug.

For the *in-vitro* drug release study, the GEM-loaded FA-CS/Fe_3O_4/GO (GEM-loaded Fe_3O_4/GO), obtained from the loading step, was transferred into a dialysis bag (MWCO 14 kDa). The bag was sealed and dipped into 50 mL of phosphate-buffered saline (PBS; pH 7.4 and 5.6) at 37 °C for 48 h. At a regular interval of time, 3 mL of solution was taken out and the same amount of fresh buffered solution was replaced to keep the volume of the release medium constant [36,37]. The amount of released GEM was determined by using a UV-Vis spectrophotometer. The release test was taken in triplicates, and the drug release percent, M_t/M_∞ (%), from GEM loaded FA-CS/Fe_3O_4/GO was quantified through Eq. (10).

$$\frac{M_t}{M_\infty}(\%) = \frac{C_t}{C_0} \times 100 \tag{10}$$

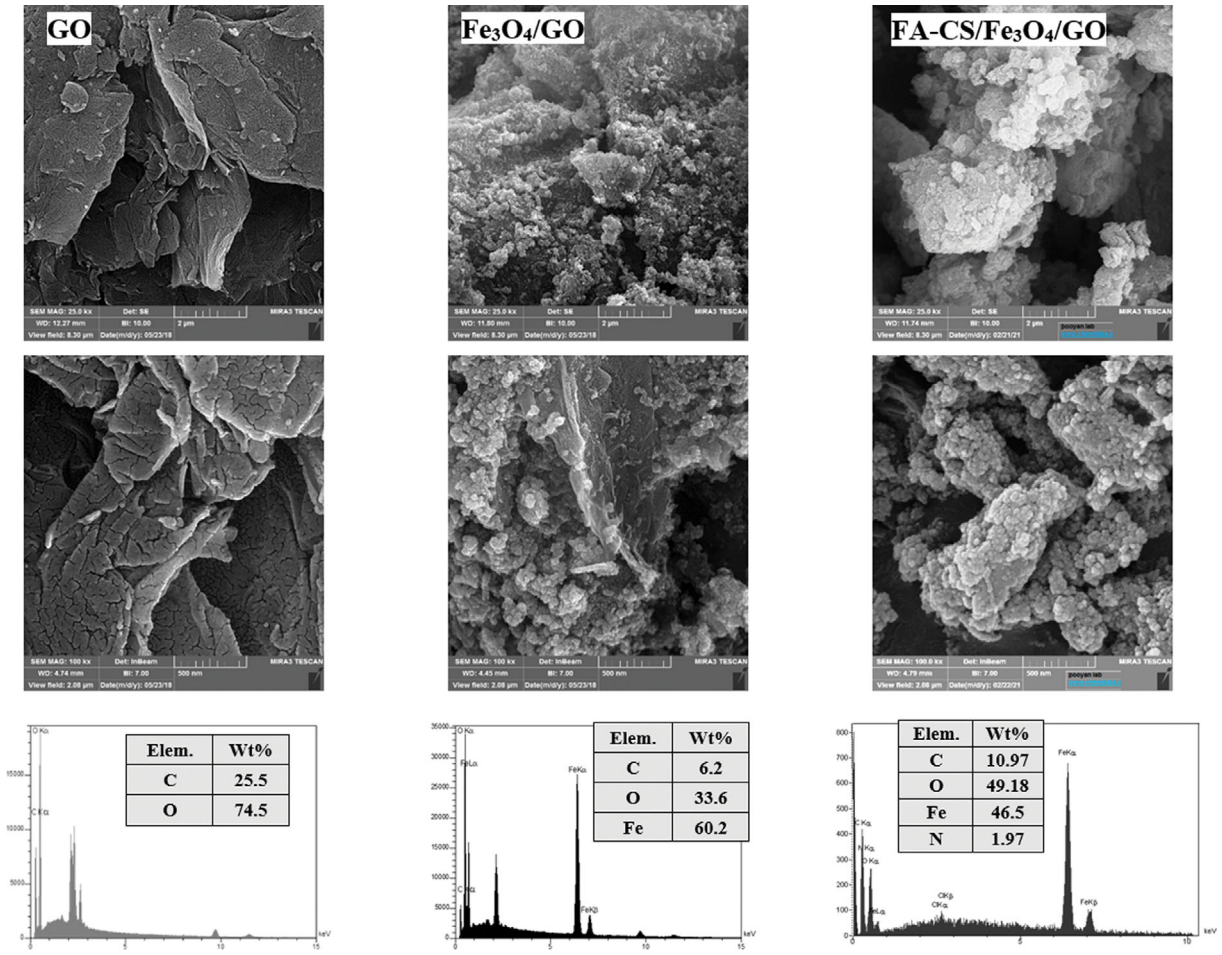

Fig. 2. FE-SEM images with low magnification (upper panels) and high magnification (middle panels), as well as the EDX spectrum (bottom panels) with the inset of elemental analysis of GO, Fe_3O_4/GO, and FA-CS/Fe_3O_4/GO.

Here, C_0 and C_t denote the quantity of GEM released and quantity of GEM loaded at time t.

7. Kinetic Release Studies

To study the kinetics of GEM release from Fe_3O_4/GO and FA-CS/Fe_3O_4/GO, the release data were analyzed based on first-order [38], Higuchi [39], Korsmeyer-Peppas [40], and Peppas-Sahlin kinetics [41]. The release kinetics of GEM can be described by Eqs. (11)-(14), respectively.

$$\frac{M_t}{M_\infty} = q_0(1-e^{-k_1 t}) \tag{11}$$

$$\frac{M_t}{M_\infty} = k_H t^{1/2} \tag{12}$$

$$\frac{M_t}{M_\infty} = k_{KP} t^n \tag{13}$$

$$\frac{M_t}{M_\infty} = k_1 t^n + k_2 t^{2n} \tag{14}$$

where q_0 is the amount of GEM released at the initial time; k_1, k_H, and k_{KP} represent the constants of the first-order, Higuchi, and Korsmeyer-Peppas kinetic models, respectively. Also, in the Peppas-Sahlin kinetic model, k_1 and k_2 are the rate constants, and n is the release exponent.

RESULTS AND DISCUSSION

1. Material Characterization

1-1. Surface Morphological Analysis

The surface morphology of GO, Fe_3O_4/GO, and FA-CS/Fe_3O_4/GO was investigated by using FE-SEM images with different magnifications. As shown in Fig. 2, the GO nanosheets have a typical wrinkled layer-like structure [42]. It is evident that a relatively large number of the non-uniform sphere-shaped Fe_3O_4 nanoparticles were decorated over the surface of GO. The SEM image of FA-CS/Fe_3O_4/GO indicates apparent changes in the surface morphology with a particle size of less than 33 nm for Fe_3O_4. Furthermore, the elemental composition of the GO, Fe_3O_4/GO, and FA-CS/Fe_3O_4/GO was determined by analyzing the surface elements using EDX. The presence of Fe signals in Fig. 2 demonstrates the existence of Fe_3O_4 on the GO sheets, and the appearance of the N peak proves the formation of CS coverage on the Fe_3O_4/GO [43]. It also shows that the percentage of C, O, N, and Fe in FA-CS/Fe_3O_4/GO is 10.97%, 49.18%, 1.97%, and 46.5%, respectively. So, the grafting of Fe_3O_4/GO with FA-CS was confirmed.

Furthermore, the inner structure of FA-CS/Fe_3O_4/GO was determined using TEM as demonstrated in Fig. 3. TEM images clearly revealed the presence of a large number of submicron Fe_3O_4 nanoparticles (the light gray spots), as well as the growth of FA-CS layer (the dark gray areas), over the transparent GO sheets.

1-2. Functional Group Analysis

The FTIR technique was adopted to identify the functional groups of the materials and the results are illustrated in Fig. 4(a). In the spectrum of GO, two typical absorbance peaks were observed around 1,390 and 1,700 cm^{-1}, which are attributed to the asymmetric and symmetric stretching vibration of -COOH and -COO- functional group, respectively. A strong peak between 500 and 600 cm^{-1} in the FT-IR spectrum of Fe_3O_4/GO can be ascribed to the Fe-O vibration mode [44]. The FA-conjugated CS exhibited a

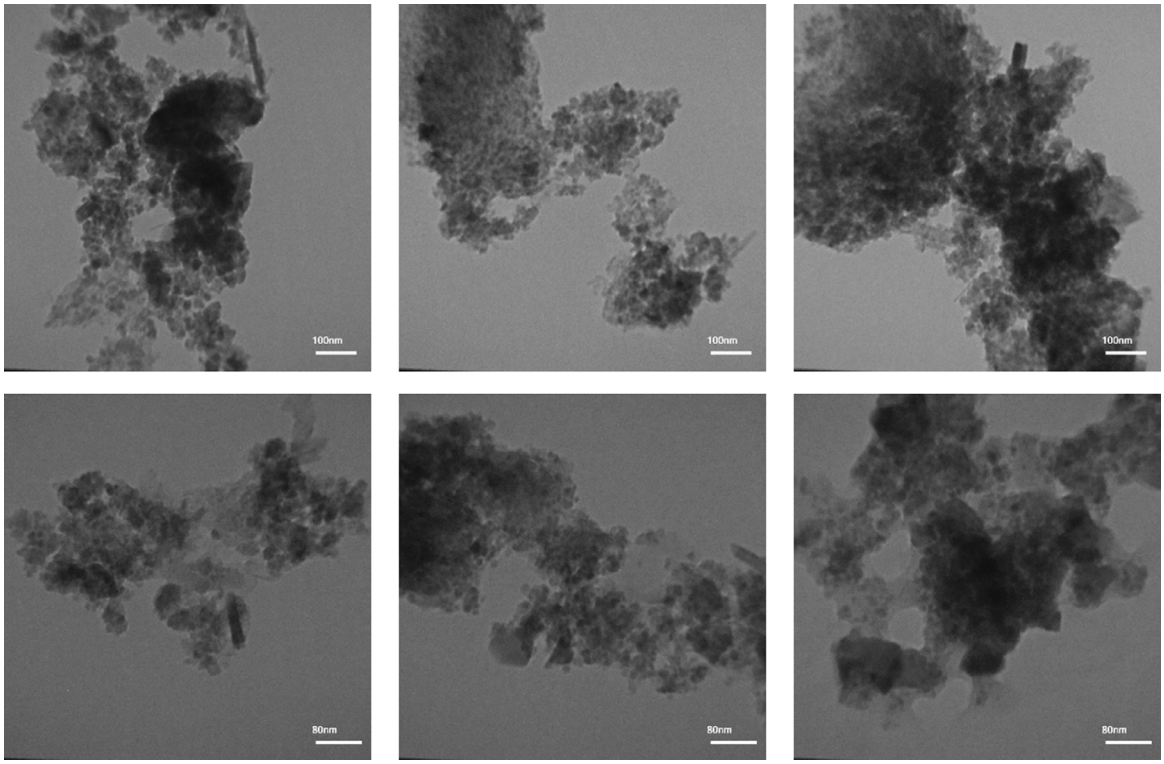

Fig. 3. TEM images of FA-CS/Fe_3O_4/GO with 100 nm (upper panels) and 80 nm (lower panels) scale bars.

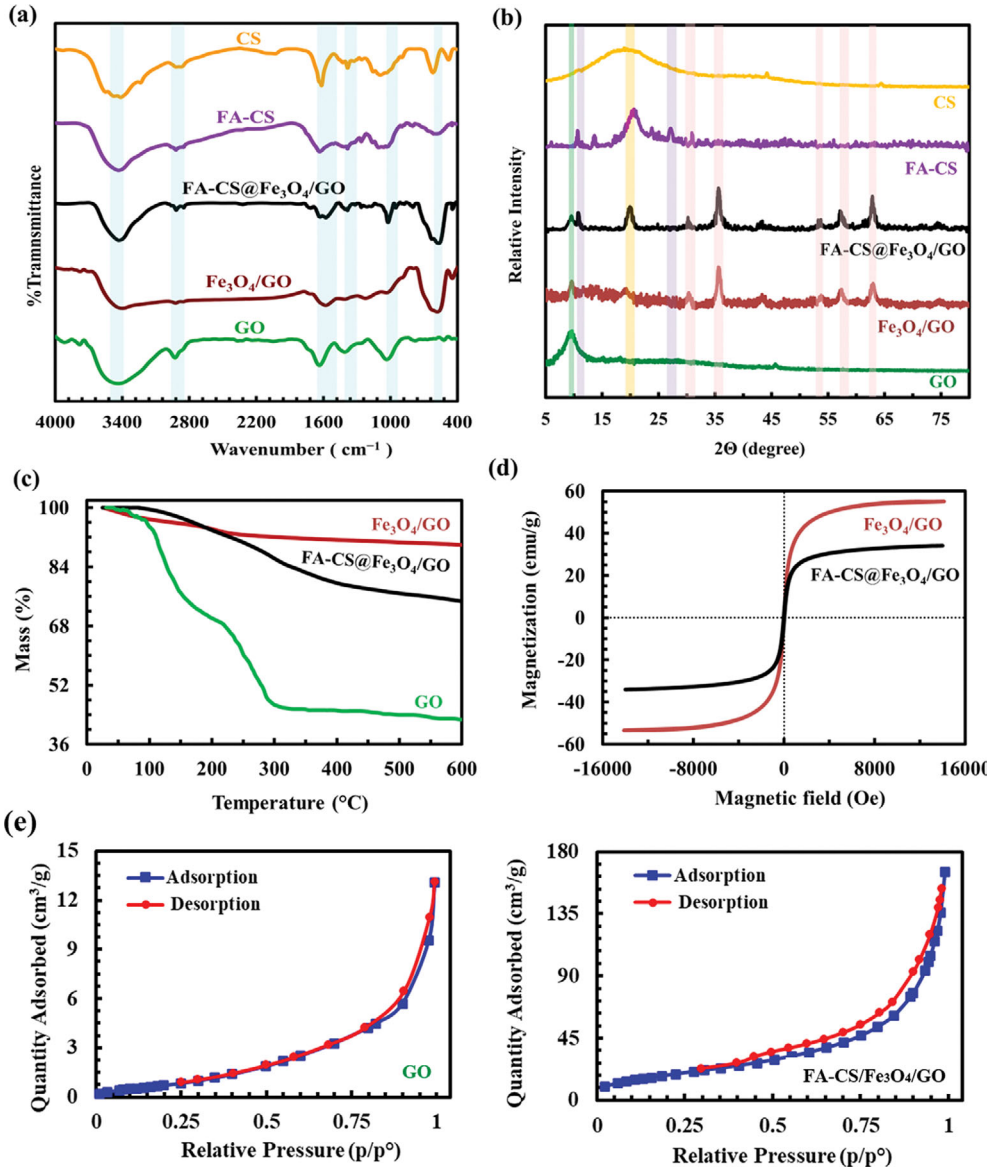

Fig. 4. (a) FT-IR spectra and (b) XRD patterns of CS, FA-CS, GO, Fe_3O_4/GO, and FA-CS/Fe_3O_4/GO; (c) TGA thermograms of GO, Fe_3O_4/GO, and FA-CS/Fe_3O_4/GO; (d) Magnetization curves of Fe_3O_4/GO and FA-CS/Fe_3O_4/GO; (e) N_2 adsorption-desorption isotherm (77 K) of GO and FA-CS/Fe_3O_4/GO.

major adsorption peak at 1,631 cm^{-1}, corresponding to the flexural vibration of the CO-NH group [45], which probably originates from the amide bond formation between free-amine groups of CS (1,624 cm^{-1}) and the carboxyl of FA (1,700 cm^{-1}). After the formation of FA-CS/Fe_3O_4/GO, all the sharp peaks of Fe_3O_4, GO, FA, and CS appeared with some slight changes in position and intensity, suggesting the successful preparation of Fe_3O_4/GO and the efficacious attachment of FA-CS into Fe_3O_4/GO.

1-3. X-ray Diffraction Analysis

XRD patterns of GO, Fe_3O_4/GO, CS, FA-CS, and FA-CS/Fe_3O_4/GO in the 2θ=2°-80° are represented in Fig. 4(b). In the XRD pattern of GO, a sharp principal diffraction peak at the 2θ value of 12° (002) is related to GO nanosheets [46,47]. In the XRD pattern of the Fe_3O_4/GO, the characteristic peaks, that appeared in the 2θ=30°, 35°, 43°, 57°, and 63°, correspond to (332), (400), (311), (220), and (440) planes of Fe_3O_4 (JCPDS -153382) [48]. A broad reflection peak at 2θ=19° supports the amorphous nature of CS polymer [49,50]. For FA-CS, two apparent peaks observed at 2θ values of 11.08° and 19.0° are typical in FA and CS XRD patterns. All the characteristic peaks of these materials emerged in FA-CS/Fe_3O_4/GO, reflecting the successful preparation of the nanocomposite.

1-4. Thermogravimetric Analysis

To investigate the thermal behavior of GO, Fe_3O_4/GO, and FA-CS/Fe_3O_4/GO, TGA was carried out with a heating rate of 10 °C min^{-1} in an N_2 atmosphere. The obtained curves are shown in Fig. 4(c). For all materials, the mass loss below 150 °C is associated with the vaporization of adsorbed moisture and solvents. The

Table 1. BET Surface Area (S_{BET}), average pore size, and total pore volume of prepared materials

Adsorbents	S_{BET} (m^2/g)	Average pore diameter (nm)	Pore volume (cm^3/g)
GO	3.54	19.31	0.017
FA-CS/Fe_3O_4/GO	68.97	14.78	0.25

TGA curve of GO exhibits two mass losses: the first at around 200 °C, which was due to the loss of oxygen-containing groups, i.e., hydroxyl, epoxy, and carboxylic groups, and the other above 411 °C, attributed to the decomposition of the carbon frame. Fe_3O_4/GO is thermally stable. The small mass loss above 250 °C corresponds to the degradation of oxygen-containing groups from GO. The total mass loss of GO, Fe_3O_4/GO, and FA-CS/Fe_3O_4/GO was about 57%, 10%, and 25%, respectively, in the whole temperature range studied. Therefore, the addition of the CS polymer, FA ligand, and Fe_3O_4 nanoparticles improved the thermal stability of GO [51], and it can be concluded that the FA-CS/Fe_3O_4/GO agent was thermally stable for drug delivery at the physiological temperature of the human body.

1-5. The Magnetic Property Analysis

The magnetic properties of Fe_3O_4/GO and FA-CS/Fe_3O_4/GO were considered in the field sweeping from −1,500 to 1,500 Oe at room temperature by using a VSM. The M-H hysteresis curves are shown in Fig. 4(d), where the specific saturation magnetization (M_s) was about 55.08 emu g^{-1} and 34.11 for Fe_3O_4/GO and FA-CS/Fe_3O_4/GO, respectively. The lower M_s value in FA-CS/Fe_3O_4/GO may be associated with the non-magnetic contribution of two compounds, i.e., CS and FA layer, coating magnetic GO. Based on the VSM results, drug-loaded FA-CS/Fe_3O_4/GO may be used as a magnetic responsive carrier for accumulating the drug in tumor sites with an extracorporeal magnetic field.

1-6. BET Surface Area Analysis

The porous structure of GO and FA-CS/Fe_3O_4/GO was approved by N_2 adsorption/desorption analysis at 77 K, and the obtained data are indicated in Fig. 4(e) and Table 1. According to the IUPAC classification, GO and FA-CS/Fe_3O_4/GO showed a type IV hysteresis loop. The BET surface area, total pore volume, and pore size diameter were 3.54, 68.96 m^2 g^{-1} and 0.017, 0.25 cm^3 g^{-1} and 19.31, 14.78 nm for GO and FA-CS/Fe_3O_4/GO, respectively. The reasonable specific surface area and porous structure of FA-CS/Fe_3O_4/GO favor the adsorption of GEM.

2. Adsorption Investigation

2-1. Effect of pH Solution

The effect of pH on GEM adsorption by FA-CS/Fe_3O_4/GO is presented in Fig. 5(a). For this purpose, a varied range of pH (2.5-8) was set. As shown in Fig. 5(a), the adsorption capacity decreased significantly with an increase in pH above 5. The maximum adsorption capacity occurred at pH 4.0 with a capacity of 4.6 mg g^{-1}. The value of optimum pH corresponds to data from an earlier study which was performed by Hamarat Sanlier et al. [52]. The isoelectric point of GEM was reported to be 3.6 and, therefore, it has a slight negative charge at pH 4.0 [52].

Since the point of zero charge (PZC) of an adsorbent, where negative charge equals positive charge, is an important factor to realize the mechanism involved in the adsorption process, it was

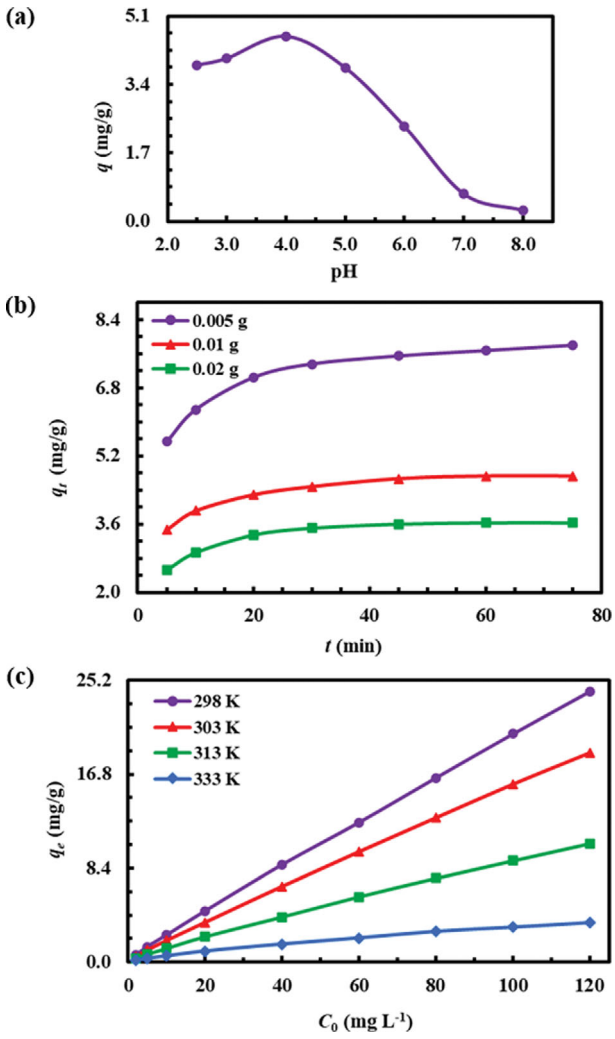

Fig. 5. (a) The effect of solution pH value on the adsorption capacity of FA-CS/Fe_3O_4/GO (Experimental conditions: adsorbent dosage=0.5 g L^{-1}, C_0=20 mg L^{-1}, temperature=298 K, and time=2 h); (b) The effects of contact time and adsorbent dosage on the adsorption capacity of FA-CS/Fe_3O_4/GO (Experimental conditions: pH=4, V=20 mL, C_0=20 mg L^{-1}, and temperature=298 K); (c) The effects of GEM initial concentration and temperature on the adsorption capacity of FA-CS/Fe_3O_4/GO (Experimental conditions: pH=4, adsorbent dosage=0.5 g L^{-1}, and time=2 h).

measured at room temperature by adding 0.05 g of FA-CS/Fe_3O_4/GO into 20 mL of 0.01 M NaCl solutions. The initial pH was adjusted using HCl or NaOH, following constant magnetic stirring at 120 rpm for 24 h. After the adsorbent material was removed, the final pH values of the solutions were measured. The intersection of the final pH *versus* initial pH plot was considered to be the

Table 2. The fitting isothermal parameters for the adsorption of GEM onto FA-CS/Fe_3O_4/GO (at 298-333 K) and Fe_3O_4/GO (at 298 K)

Isotherm models	Parameters	FA-CS/Fe_3O_4/GO				Fe_3O_4/GO
		Temperature (K)				
		298	303	313	333	298
Langmuir	q_{max} (mg g^{-1})	221.1699	136.5650	46.0911	7.7526	33.9937
	K_L (L mg^{-1})	0.0011	0.0014	0.0025	0.0069	0.0021
	R^2	0.9998	0.9998	0.9996	0.9993	0.9992
Freundlich	K_F ($mg^{1-\frac{1}{n}}L^{\frac{1}{n}}g^{-1}$)	0.3146	0.2553	0.1827	0.1142	0.1102
	n	1.0780	1.0950	1.1678	1.3861	1.1541
	R^2	0.9999	1.0000	0.9999	0.9996	0.9998
Temkin	A_T (L mg^{-1})	0.2852	0.2797	0.2832	0.3107	0.2789
	b (J g mol^{-1} mg^{-1})	454.741	593.643	1080.43	3360.980	1608.770
	R^2	0.9313	0.9336	0.9424	0.9641	0.9404
Dubinin-Radushkevich	q_S (mg m^{-1})	25.3411	19.6163	10.8701	3.2702	7.0903
	B (mol^2 J^{-2})×10^{-4}	2.7422	2.7177	2.4206	1.0984	2.9652
	E (kJ mol^{-1})	0.0427	0.0429	0.0454	0.0675	0.0411
	R^2	0.9724	0.9733	0.9706	0.9671	0.9683

pH_{PZC}. The pH_{PZC} for FA-CS/Fe_3O_4/GO was found to be nearly 4. Hence, at pH 4.0 the surface of the FA-CS/Fe_3O_4/GO was neutral and consequently GEM could not interact with the surface of the adsorbent due to their counter charges. Thus, it can be referred that GEM adsorption did not happen through electrostatic interaction. Alternately, hydrogen bonds and π-π interactions are regarded as dominant forces involved in drug uptake [47]. Similar results were reported for the 5-fluorouracil uptake by CS-functionalized GO [47] and methylene blue adsorption onto poly(acrylic acid) functionalized magnetic GO [53]. At higher pH (>4), GEM starts to become negatively charged by giving its protons to the solvent, and FA-CS/Fe_3O_4/GO loses its positive charge. As a consequence, it is expected that the adsorption process weakens and q values decline.

2-2. Effect of the Contact Time and Adsorbent Dosage

The effects of contact time and FA-CS/Fe_3O_4/GO dosage on GEM adsorption are indicated in Fig. 5(b). For these tests, the amounts of FA-CS/Fe_3O_4/GO and contact time in a range of 5-20 mg and 2-75 min were studied, respectively. The adsorption capacity of the adsorbent for GEM increased very fast within 30 min, slightly after 30 min and the adsorption capacity of GEM was almost constant [54]. The adsorption capacity for GEM at 75 min was estimated to be 3.62, 4.73, and 7.80 mg g^{-1} using 5, 10, and 20 mg of FA-CS/Fe_3O_4/Go at pH 4 and room temperature, respectively. Thus, decreased FA-CS/Fe_3O_4/GO dosage resulted in increased adsorption capacity of GEM [55].

2-3. Effect of the Initial Drug Concentration and Temperature

The concentration of FA-CS/Fe_3O_4/GO and temperature could directly affect the adsorption capacity of GEM. Different initial concentrations of GEM (2-120 mg L^{-1}) were estimated for adsorption of drug from aqueous solution at 298-333 K. As presented in Fig. 5(c), the adsorption capacity reached the maximum value when the concentration of GEM was 120 mg L^{-1} at 298 K. As the initial concentration of GEM was increased, the adsorption capacity of GEM increased because of the higher number of GEM molecules in the solution [56]. Moreover, the data showed that a temperature of 298 K was sufficient to fulfill the adsorption process.

3. Adsorption Isotherms and Kinetics

The adsorption isotherm of FA-CS/Fe_3O_4/GO for GEM was studied at four different temperatures. The results were evaluated by the non-linear Langmuir, Freundlich, Temkin, and Dubinin-Radushkevich equations, respectively. The isotherm parameters of the adsorption isotherm were calculated and listed in Table 2. As observed from this table, the adsorption capacity, q_{max}, of GEM onto FA-CS/Fe_3O_4/GO are 221.17, 136.56, 46.09, and 7.75 mg g^{-1} at 298, 303, 313, and 333 K, respectively. By increasing the temperature, adsorption capacity values were decreased, which implied that GEM adsorption has an exothermic nature. The q_{max} value of GEM was 221.17 mg g^{-1} for FA-CS/Fe_3O_4/GO, which is much greater than the 33.99 mg g^{-1} obtained using unmodified Fe_3O_4/GO at 298 K. The increment in the amount of q_{max} caused by the grafting of magnetic GO with FA-CS.

The regression coefficients (R^2) for the Freundlich isotherm models are higher than 0.999 (Table 2), signifying that the Freundlich model is more proper to describe the adsorption behavior than other models. Thus, it can be concluded that the multilayer adsorption process of GEM takes place at binding sites on the heterogeneous surface of both adsorbents with variable energy levels. Moreover, the magnitude of the Freundlich exponent (n) at all temperatures was greater than 1, implying that the interaction force between GEM and adsorbents was favorable and strong [57].

To investigate the adsorption rate, for commonly used non-linear kinetic models, the PSO, the PFO, Elovich, and FP, were used to analyze the modeling of the experimental data [58]. The kinetic models at three adsorbent dosages (i.e., 5, 10, and 20 mg) and the calculated kinetic parameters were tabulated in Table 3. As can be seen in Table 3, by increasing the adsorbent dosage, the $q_{e,cal}$ value for the PSO kinetic models was decreased. Also, the R^2 value of

Table 3. The fitting kinetic parameters for the adsorption of GEM onto different dosages of FA-CS/Fe_3O_4/GO

Kinetics models	Parameters	Adsorbent dosage (mg)		
		5	10	20
Pseudo-1st-order	k_1 (min^{-1})	0.2391	0.2633	0.2257
	$q_{e,cal}$ (mg g^{-1})	7.4569	4.5146	3.5075
	R^2	0.9981	0.9980	0.9984
Pseudo-2nd-order	k_2 (g $mg^{-1}min^{-1}$)	0.0537	0.0979	0.1003
	$q_{e,cal}$ (mg g^{-1})	7.9459	4.8314	3.7894
	R^2	0.9999	0.9998	0.9999
Simplified Elovich	α (mg $g^{-1}min^{-1}$)	156.175	97.0934	27.038
	β (g mg^{-1})	1.2015	1.9430	2.1860
	R^2	0.9996	0.9998	0.9994
Fractional Power	a (mg $g^{-1}min^{b}$)	4.7619	2.9230	2.1064
	b	0.1194	0.1222	0.1410
	R^2	0.9994	0.9997	0.9991
	$q_{e,exp}$ (mg g^{-1})	7.7987	4.7319	3.5962

the PSO model was somewhat higher than that of other kinetic models. Therefore, the PSO kinetics model is more appropriate to describe the adsorption behavior of GEM onto FA-CS/Fe_3O_4/GO. The adsorption rate constant in the PSO model, k_2, increased with the increasing adsorbent dosage (Table 3).

4. Release Kinetics

Designing drug delivery systems with pH-responsiveness features provides an efficient manner to control drug release behavior through pH variations in order to maximize treatment efficiency on cancer cells while minimizing side effects on normal cells. Because cancer cells cause the pH environment to decrease to more acidic values compared to healthy cells, release studies were performed in the simulated cancer fluid (SCF, pH 5.6) and simulated blood fluid (SBF, pH 7.4) for the prepared carriers as a GEM delivery system [59]. Fig. 6 displays the *in-vitro* release profile of GEM from the drug-loaded Fe_3O_4/GO and FA-CS/Fe_3O_4/GO during a period of 48 h at 37 °C. During the first 60 min, 11.31% and 13.06% of GEM loaded Fe_3O_4/GO were released at pH 5.6 and 7.4, respectively. While for FA-CS/Fe_3O_4/GO, the amount of GEM released was 18.65% and 12.39% after 60 min in the medium with pH 5.6 and 7.4, respectively. The amount of the released GEM from Fe_3O_4/GO was 33.98% and 39.23% after 48 h at pH 5.6 and 7.4, respectively. After the grafting of Fe_3O_4/GO with FA-CS, GEM release reached 83.4% and 58.11% within 48 h in the medium with pH 5.6 and 7.4, respectively. As can be seen in Fig. 6, the drug release from both carriers, particularly for FA-CS/Fe_3O_4/GO, at the slightly acidic pH is higher compared to pH 7.4. GEM release increased at pH 5.6 due to a weakening of the π-π stacking interaction between the GEM drug and carriers. According to the obtained drug release results, GEM shows superior releasing power from the FA-CS/Fe_3O_4/GO nanocomposite as compared to the non-functionalized Fe_3O_4/GO in terms of availability in the SCF medium for the extended time periods (48 h).

To further achieve the mathematical information of release rate of GEM from FA-CS/Fe_3O_4/GO and Fe_3O_4/GO, first-order, Higuchi, Korsmeyer-Peppas and Peppas-Sahlin kinetic models were

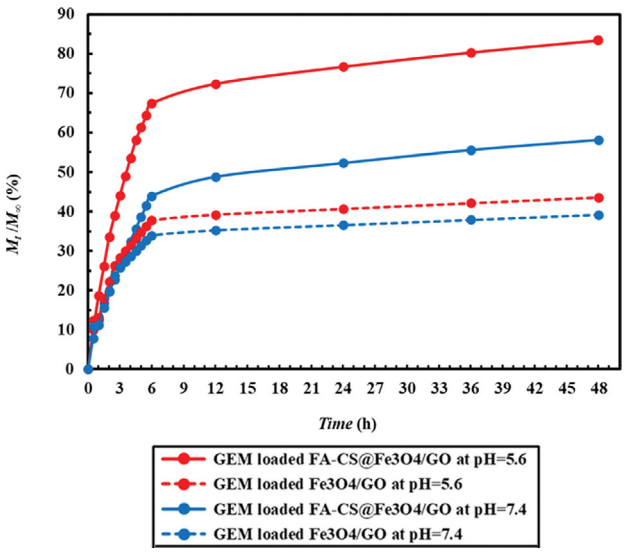

Fig. 6. Release plots of GEM from FA-CS/Fe_3O_4/GO and Fe_3O_4/GO in 0.9 g L^{-1} PBS of two pH values (5.6 and 7.4) at 37 °C.

used [37,60]. The non-linear plots obtained from the models were depicted in Fig. 7 as a cumulative drug release percentage at time *t* vs. The values of the parameters of each analytical equation are listed in Table 4. According to the R^2 values, the Korsmeyer-Peppas model seemed to be a more suitable kinetic model for both Fe_3O_4/GO and FA-CS/Fe_3O_4/GO, respectively. If n=0.5 or n≤0.5, drug diffusion is Fickian, for 0.5<n<1, drug diffusion is non-Fickian, for n=1, drug diffusion is non-Fickian (case II transport), for n>1, attributed to super case II transport [38]. The n values show that the GEM release mechanisms for both of the carriers is non-Fickian diffusion (Table 4).

CONCLUSIONS

A pH- and magnetic field-responsive system was prepared by

Table 4. The fitting kinetic parameters for the cumulative release of GEM from FA-CS/Fe_3O_4/GO and Fe_3O_4/GO in PBS at 37 °C

Kinetics models	Parameters	FA-CS/Fe_3O_4/GO		Fe_3O_4/GO	
		pH value			
		5.6	7.4	5.6	7.4
First-order	k_1 (min^{-1})	0.2258	0.1779	0.4267	0.4071
	q_0 (mg g^{-1})	90.5974	65.5377	39.5886	36.3092
	R^2	0.9999	0.9984	0.9971	0.9973
Higuchi	k_H ($min^{-1/2}$)	26.1171	16.285	15.6772	14.1088
	R^2	0.9918	0.9907	0.9984	0.9979
Korsmeyer-Peppas	K_{KP} (min^{-n})	20.2145	12.091	15.7020	13.8330
	n	0.6889	0.7181	0.4988	0.5148
	R^2	0.9992	0.9998	0.9984	0.9979
Peppas-Sahlin	K_1 (min^{-n})	20.0662	9.5507	16.7811	14.6694
	K_2 (min^{-2n})	−1.318	2.8306	−1.5002	−1.4063
	n	0.8975	0.5348	0.6336	0.6920
	R^2	0.9999	0.9999	0.9986	0.9983

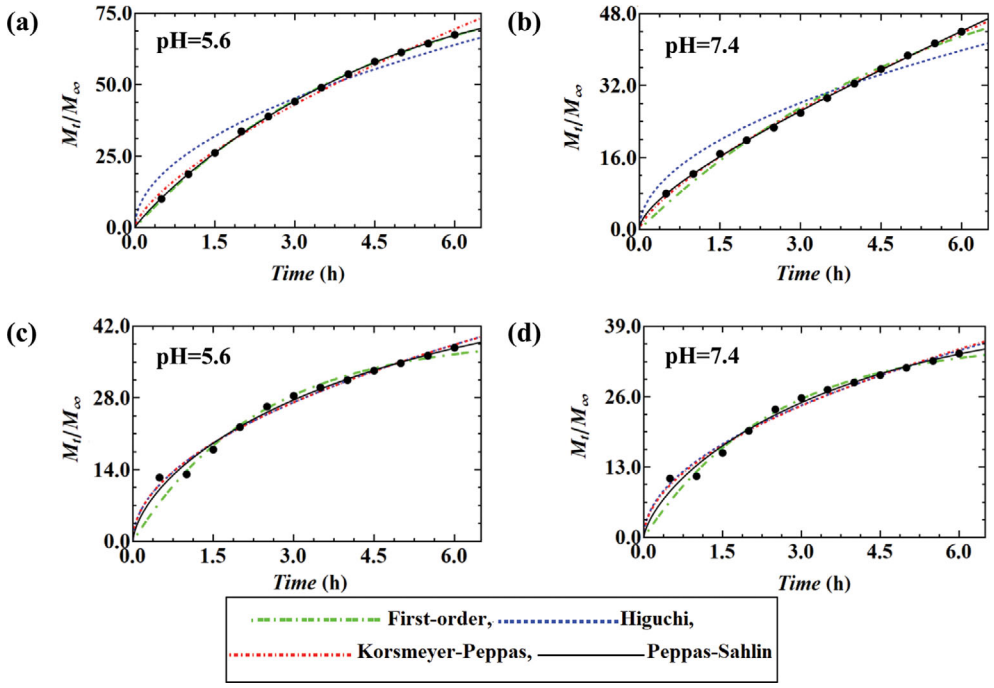

Fig. 7. Non-linear fitting plots of kinetic models for the cumulative release of GEM from FA-CS/Fe_3O_4/GO (a), (b) and Fe_3O_4/GO (c), (d) in PBS of pH 5.6 and 7.4 at 37 °C. The black circles show experimental data.

grafting FA-CS on the Fe_3O_4/GO for potential application in drug delivery. The FA-CS/Fe_3O_4/GO nanocomposite demonstrated high surface area, porous structure, and superparamagnetic behavior with the saturation M_s value of 34.11 emu g^{-1}. In the adsorption studies, the optimum pH value was determined as pH of 4, the adsorbent dosage of 0.5 g L^{-1}, contact time of 45 min, and temperature of 298 K. The adsorption kinetics followed the PSO model, and the equilibrium data were well fitted by the Freundlich isotherm. For FA-CS/Fe_3O_4/GO, the total amount of GEM released was about 83.4% under SCF conditions, whereas only 58.11% of GEM was released at SBF conditions within 48 h. The obtained higher availability of the GEM at pH 5.6 than pH 7.4 is valuable in chemotherapy and suggests that the GEM-loaded FA-CS/Fe_3O_4/GO may be a promising candidate in cancer treatment.

SUPPORTING INFORMATION

Additional information as noted in the text. This information is available via the Internet at http://www.springer.com/chemistry/journal/11814.

REFERENCES

1. X. Fang, J. Cao and A. Shen, *J. Drug Deliv. Sci. Technol.*, **57**, 101662 (2020).
2. F. U. Din, W. Aman, I. Ullah, O. S. Qureshi, O. Mustapha, S. Shafique and A. Zeb, *Int. J. Nanomedicine*, **12**, 7291 (2017).
3. S. Hossen, M. K. Hossain, M. K. Basher, M. N. H. Mia, M. T. Rahman and M. J. Uddin, *J. Adv. Res.*, **15**, 1 (2019).
4. B. D. Kevadiya, G. V. Joshi, H. A. Patel, P. G. Ingole, H. M. Mody and H. C. Bajaj, *J. Biomater. Appl.*, **25**, 161 (2010).
5. A. Z. Juthi, M. Aquib, M. A. Farooq, S. Ghayas, F. Khalid, G. F. Boafo, D. P. Wande, D. H. Khan, T. Z. Bithi, R. Bavi and B. Wang, *Environ. Chem. Lett.*, **18**, 1509 (2020).
6. P. Makvandi, M. Ghomi, M. Ashrafizadeh, A. Tafazoli, T. Agarwal, M. Delfi, J. Akhtari, E. N. Zare, V. V. T. Padil, A. Zarrabi, N. Pourreza, W. Miltyk and T. K. Maiti, *Carbohydr. Polym.*, **250**, 116952 (2020).
7. A. A. Ghawanmeh, G. A. M. Ali, H. Algarni, S. M. Sarkar and K. F. Chong, *Nano Res.*, **12**, 973 (2019).
8. S. Gooneh-Farahani, M. R. Naimi-Jamal and S. M. Naghib, *Expert. Opin. Drug Deliv.*, **16**, 79 (2018).
9. S. W. Jun, P. Manivasagan, J. Kwon, V. T. Nguyen, S. Mondal, C. D. Ly, J. Lee, Y. H. Kang, C. S. Kim, and J. Oh, *Int. J. Biol. Macromol.*, **155**, 961 (2020).
10. C. Chen, W. Yao, W. Sun, T. Guo, H. Lv, X. Wang, H. Ying, Y. Wang and P. Wang, *Int. J. Biol. Macromol.*, **122**, 1090 (2019).
11. S. Karki, M. B. Gohain, D. Yadav and P. G. Ingole, *Int. J. Biol. Macromol.*, **193**, 2121 (2021).
12. P. G. Ingole and N. P. Ingole, *Korean J. Chem. Eng.*, **31**, 2109 (2014).
13. F. Xu, T. Zhao, T. Yang, L. Dong, X. Guan and X. Cui, *Colloids Surf. A Physicochem. Eng. Asp.*, **490**, 22 (2016).
14. P. Ebrahimnejad, A. Sodagar Taleghani, K. Asare-Addo and A. Nokhodchi, *Drug Discov. Today*, **27**, 471 (2022).
15. P. Dramou, M. Fizir, A. Taleb, A. Itatahine, N. S. Dahiru, Y. A. Mehdi, L. Wei, J. Zhang and H. He, *Carbohydr. Polym.*, **197**, 117 (2018).
16. P. Pakdaman Goli, M. Bikhof Torbati, K. Parivar, A. Akbarzadeh Khiavi and M. Yousefi, *J. Drug Deliv. Sci. Technol.*, **65**, 102756 (2021).
17. A. Deb and R. Vimala, *J. Drug Deliv. Sci. Technol.*, **43**, 333 (2018).
18. M. De Sousa, L. A. Visani De Luna, L. C. Fonseca, S. Giorgio and O. L. Alves, *ACS Appl. Nano Mater.*, **1**, 922 (2018).
19. Z. Wang, C. Zhou, J. Xia, B. Via, Y. Xia, F. Zhang, Y. Li and L. Xia, *Colloids Surf. B Biointerfaces*, **106**, 60 (2013).
20. H. Hu, C. Tang and C. Yin, *Mater. Lett.*, **125**, 82 (2014).
21. K. Vinothini, N. K. Rajendran, A. Ramu, N. Elumalai and M. Rajan, *Biomed. Pharmacother.*, **110**, 906 (2019).
22. B. K. Purushothaman, M. Harsha S, P. U. Maheswari and K. M. M. Sheriffa Begum, *J. Drug Deliv. Sci. Technol.*, **52**, 509 (2019).
23. K. Krishnamoorthy, G. S. Kim and S. J. Kim, *Ultrason. Sonochem.*, **20**, 644 (2013).
24. S. E. Rokni, R. Haji Seyed Mohammad Shirazi, M. Miralinaghi and E. Moniri, *Res. Chem. Intermed.*, **46**, 2247 (2020).
25. M. Shafaati, M. Miralinaghi, R. H. S. M. Shirazi and E. Moniri, *Res. Chem. Intermed.*, **46**, 5231 (2020).
26. I. Langmuir, *J. Am. Chem. Soc.*, **40**, 1361 (1918).
27. H. M. F. Freundlich, *Z. Phys. Chem.*, **57**, 385 (1906).
28. M. I. Temkin and V. Pyzhev, *Acta Phys. Chim. USSR*, **12**, 327 (1940).
29. M. M. Dubinin and L. V. Radushkevich, *Proc. Acad. Sci. USSR Phys. Chem. Sect.*, **55**, 331 (1947).
30. S. Lagergren, *Sven. Veten. Handl.*, **24**, 1 (1898).
31. Y. S. Ho and G. McKay, *Process Biochem.*, **34**, 451 (1999).
32. I. S. McLintock, *Nature*, **216**, 1204 (1967).
33. Y. S. Ho and G. McKay, *Adsorp. Sci. Technol.*, **20**, 797 (2002).
34. S. Alharthi and M. O. A. El-Magied, *Korean J. Chem. Eng.*, **38**, 2365 (2021).
35. A. Hashem, C. O. Aniagor, S. M. Badawy and G. M. Taha, *Korean J. Chem. Eng.*, **38**, 2256 (2021).
36. S. P. Hooshyar, R. Z. Mehrabian, H. A. Panahi, M. H. Jouybari and H. Jalilian, *Colloids Surf. B Biointerfaces*, **176**, 404 (2019).
37. N. Torabi Fard, F. Tadayon, H. Ahmad Panahi and E. Moniri, *J. Mol. Liq.*, **349**, 118149 (2021).
38. S. Dash, P. N. Murthy, L. Nath and P. Chowdhury, *Acta Pol. Pharm.*, **67**, 217 (2010).
39. T. Higuchi and N. York, *J. Pharm. Sci.*, **52**, 1145 (1963).
40. R. W. Korsmeyer, R. Gurny, E. Doelker, P. Buri and N. A. Peppas, *Int. J. Pharm.*, **15**, 25 (1983).
41. N. A. Peppas and J. J. Sahlin, *Int. J. Pharm.*, **57**, 169 (1989).
42. E. Aliyari, A. A. Fathi, M. Alvand, P. Jamshidi, F. Shemirani, S. Mozaffari and M. R. Neyestani, *Res. Chem. Intermed.*, **47**, 1905 (2021).
43. A. Homayonfard, M. Miralinaghi, R. H. S. M. Shirazi and E. Moniri, *Water Sci. Technol.*, **78**, 2297 (2018).
44. Y. B. Kontaş, E. Erçarıkcı and M. Alanyalıoğlu, *Res. Chem. Intermed.*, **47**, 3853 (2021).
45. P. G. Ingole, H. C. Bajaj and K. Singh, *Arab. J. Chem.*, **9**, S960 (2016).
46. P. Khorshidi, R. H. S. M. Shirazi, M. Miralinaghi, E. Moniri and S. Saadi, *Res. Chem. Intermed.*, 1 (2020).
47. P. Miralinaghi, P. Kashani, E. Moniri and M. Miralinaghi, *Mater. Res. Express*, **6**, 065305 (2019).
48. P. Jamshidi and F. Shemirani, *Res. Chem. Intermed.*, **46**, 4403 (2020).
49. A. I. Adeogun, O. A. Osideko, M. A. Idowu, V. Shappur, O. A. Akinloye and B. Ramesh Babu, *SN Appl. Sci.*, **2**, 795 (2020).
50. H. Ansari, M. Miralinaghi and F. Azizinezhad, *Cellul. Chem. Technol.*, **53**, 191 (2019).
51. L. Hou, C. Yang, X. Rao, L. Hu, Y. Bao, Y. Gao and X. Zhu, *Colloids Surf. A Physicochem. Eng. Asp.*, **625**, 126949 (2021).
52. S. Hamarat Sanlıer, M. Yasa, A. O. Cihnioglu, M. Abdulhayoglu, H. Yılmaz and G. Ak, *Artif. Cells, Nanomedicine, Biotechnol.*, **44**, 943 (2016).
53. J. Zhang, M. S. Azam, C. Shi, J. Huang, B. Yan, Q. Liu and H. Zeng, *RSC Adv.*, **5**, 32272 (2015).
54. A. Barazandeh, H. A. Jamali and H. Karyab, *Korean J. Chem. Eng.*, **38**, 2436 (2021).
55. S. Karimidost, E. Moniri and M. Miralinaghi, *Korean J. Chem. Eng.*, **36**, 1115 (2019).
56. M. A. A. Marhalim, S. S. Mohtar, A. M. Mohammed, F. Aziz, M. N. M. Sokri, W. N. W. Salleh, N. Yusof, J. Jaafar, A. F. Ismail, M. Aziz and R. Naim, *Korean J. Chem. Eng.*, **38**, 1648 (2021).
57. L. Sun, S. Hu, H. Sun, H. Guo, H. Zhu, M. Liu and H. Sun, *RSC Adv.*, **5**, 11837 (2015).
58. W. Janusz, V. Sydorchuk, E. Skwarek, S. Khalameida, J. Skubiszewska-Zięba and R. Leboda, *Appl. Nanosci.*, **1**, 1 (2021).
59. C. Lim, E. B. Cho and D. Kim, *Korean J. Chem. Eng.*, **36**, 166 (2019).
60. S. F. Kaboli, F. Mehrnejad and A. Nematollahzadeh, *J. Drug Deliv. Sci. Technol.*, **64**, 102588 (2021).